energies

MDPI

Article

Energy-Aware WLAN Deployment for Operational Energy and Carbon Reduction in Multi-Story Public Buildings

Mustafa Coşar

Department of Computer Engineering, Hitit University, 19030 Çorum, Türkiye; mustafacosar@hitit.edu.tr

Abstract

The energy consumption of digital communication infrastructures is increasingly recognized as a component of operational building energy use. In multi-story public buildings, Wireless Local Area Networks (WLANs) are typically deployed under static, always-on configurations, leading to avoidable energy overhead caused by spatial interference and inefficient access point placement. This study proposes an energy-aware WLAN deployment framework that integrates user-weighted spatial placement with deterministic three-dimensional vertical interference coordination. The framework is evaluated using 50 independent Monte Carlo simulations on a representative three-story public building model. Results indicate a reduction in annual operational energy consumption from 1892.71 kWh to 1333.71 kWh (-29.5%), with a proportional decrease in carbon emissions, while maintaining a 97% coverage requirement. Furthermore, worst-case signal quality improves, with Signal-to-Interference-plus-Noise Ratio (SINR) P10 increasing from 17.66 dB to 25.53 dB and median network capacity rising by 30.6%. These findings suggest that interference-aware spatial coordination can function as an effective energy optimization layer within building-integrated digital infrastructures.

Keywords: building energy systems; energy-aware networking; WLAN deployment; inter-floor interference; operational carbon emissions; access point placement

1. Introduction

The digital transformation of public services has fundamentally altered the operational energy profile of modern buildings. Wireless Local Area Networks (WLANs) have evolved from auxiliary systems to critical, always-on infrastructures that significantly contribute to institutional electricity demand [1–5]. While energy efficiency is well-established in cellular networks [6–9] and large-scale telecom systems [8,10], building-scale WLAN deployments are rarely analyzed as active components of the built environment's energy ecosystem. Previous research typically treats network infrastructure and building energy performance—such as Heating, Ventilation, and Air Conditioning (HVAC) and lighting—as separate domains [1,2,11].

Current building energy optimization frameworks largely overlook network topology [12,13]. This is a critical omission because indoor wireless propagation is governed by architectural geometry and materials [14–18]. In multi-story public buildings, the standard vertical alignment of Access Points (APs) exacerbates inter-floor Co-Channel Interference (CCI) [19–21]. This structural interference degrades the Signal-to-Interference-plus-Noise Ratio (SINR) even when signal strength remains adequate, leading to spectral inefficiencies [22–24].

Check for updates

Academic Editors: Julian Wang, Yanxiao Feng and Nan Wang

Received: 12 February 2026
Revised: 15 April 2026
Accepted: 21 April 2026
Published: 24 April 2026

Copyright: © 2026 by the author. Licensee MDPI, Basel, Switzerland. This article is an open access article distributed under the terms and conditions of the Creative Commons Attribution (CC BY) license.

Traditional WLAN planning prioritizes coverage [25,26] or relies on hardware-level strategies like transmit power control and sleep modes [27–30]. Although recent studies on 802.11ax [31] and Machine Learning-based propagation modeling [32–34] have improved channel characterization, they often lack integration with operational carbon metrics. Furthermore, while BIM-enabled frameworks are emerging [35–37], a research gap persists at the intersection of material-aware propagation, occupant-weighted demand, and operational carbon optimization in multi-story environments.

To address this gap, the primary purpose of this study is to reframe WLAN planning in multi-story public buildings from a purely connectivity-driven layout problem to a building-integrated energy and carbon optimization problem. To achieve this, this study proposes an Energy-Aware WLAN Deployment Framework combining a User-Weighted Spatial (WS) placement model with a deterministic Vertical Staggering Algorithm (VSA). Unlike static, coverage-first deployments that often lead to over-provisioning and high operational energy waste, this framework aligns AP placement with functional occupancy zones and intentionally staggers vertical coordinates in 3D space to mitigate structured CCI.

Through Monte Carlo simulations on a representative three-story public building, this study demonstrates that optimizing spectral efficiency fundamentally translates into measurable reductions in annual electricity consumption and carbon emissions, thereby supporting "Zero-Emission" building targets. The primary contributions are:

- A user-WS placement mechanism aligning AP deployment with functional demand zones;
- A deterministic 3D vertical staggering strategy mitigating structured inter-floor CCI;
- An integrated evaluation framework linking WLAN topology to spectral efficiency and operational carbon footprint.

By bridging wireless communication optimization with building energy sustainability, this study contributes to the emerging paradigm of digitally integrated, low-carbon public buildings.

2. Materials and Methods

This study treats WLAN planning in multi-story public buildings as an integrated operational optimization problem. The proposed WS–VSA framework comprises three coupled layers: (i) functional spatial representation, (ii) demand-driven Access Point (AP) placement, and (iii) three-dimensional (3D) inter-floor interference coordination. Network performance metrics are directly mapped to annual electricity use and operational carbon emissions to enable energy-centric comparisons [3,38].

2.1. Functional Graph-Based Building Representation

The building is modeled as a 3D functional spatial graph, $G = (V, E)$, to support deterministic AP coordination across floors.

- **Nodes** (V)**:** Each node $v_i \in V$ represents a functional zone (e.g., classroom, office) positioned at its geometric centroid $p_i = (x_i, y, z_i)$.
- **Weighting** (w_i)**:** A dynamic demand weight w_i is assigned to each node based on zone usage and traffic density, as detailed in Section 2.2.
- **Edges** (E)**:** Edges $e_{ij} \in E$ denote spatial adjacency, annotated with material-dependent Wall Attenuation Factors (WAF). The propagation follows a log-normal path loss model extended with multi-wall and inter-floor terms [19,20].
- **Vertical Stratification:** Floors are modeled as stacked layers separated by height h, explicitly accounting for inter-floor leakage and structured CCI [14,22].

Table 1 outlines the physical and structural parameters of the reference building, representing a typical reinforced concrete public facility.

Table 1. Physical and structural parameters of the reference building.

Parameter	Value/Description
Building Topology	Standard Multi-Story Public Service Building
Total built-up area	~3600 m^2
Number of floors	3
Floor-to-floor height	3.5 m
Floor Layout	Symmetrical 16-unit grid per floor block
External wall material	Reinforced concrete (25 cm)
Internal partition material	Brick masonry/hollow clay tile (15 cm)
Floor slab material	Reinforced concrete
WAF (external wall)	12–15 dB
WAF (internal wall)	4–6 dB
Floor slab attenuation	18–25 dB
Log-normal Path Loss Exponent (η)	2.8–3.2 (Indoor mixed environment)

Material parameters and WAF values align with ITU-R recommendations [19] to ensure physical realism. The log-normal path loss exponent (η = 2.8–3.2) reflects mixed indoor environments with moderate structural segmentation. All physical and propagation-related parameters were held constant across simulation scenarios to ensure controlled comparison between the baseline corridor-aligned deployment and the proposed energy-aware WS–VSA strategy.

Figure 1 represents the mathematical model of a standard public service building and the functional zones that form the basis for WLAN placement optimization. The model treats the building not just as a geometric space, but as a Functional Signal Graph weighted according to user density and service type.

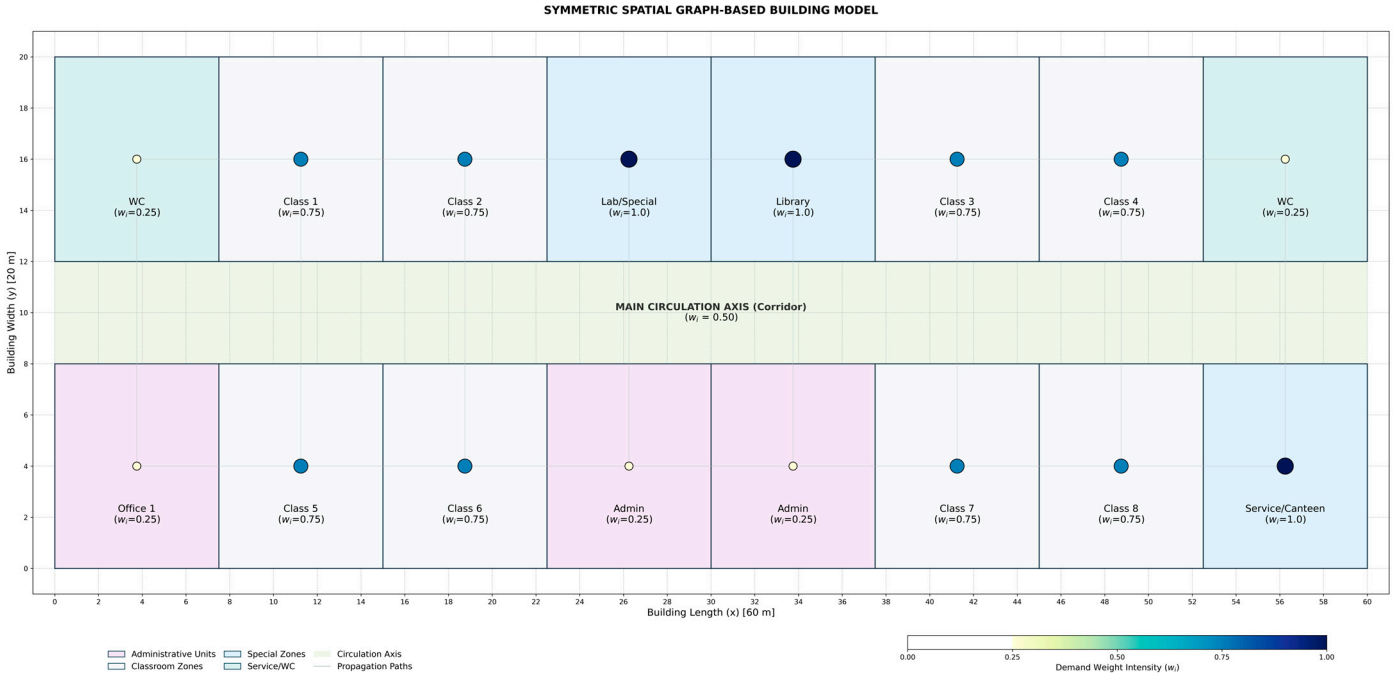


Figure 1. Functional Graph-Based Representation and Spatial Demand Weighting of the Reference Building (generated by the author using Python, version 3.13.9, Python Software Foundation, Wilmington, DE, USA).

2.2. User-Centric Demand Weighting Model

To account for non-uniform occupancy in public buildings, each demand node is assigned a normalized functional demand weight $w_i \in (0, 1]$ computed as:

$$w_i = K \cdot \frac{(U_i \cdot D_i)}{\max_i (U_i \cdot D_i)} \quad (1)$$

where U_i is the expected concurrent user count in zone i, D_i is the normalized service demand coefficient, and K is a normalization constant. This weighting layer ensures digital infrastructure tracks operational demand rather than remaining uniformly overprovisioned [3,39].

The normalization process in Equation (1) ensures that demand weights satisfy $0 < w_i \leq 1$, enabling scale-independent comparison among heterogeneous functional zones. This formulation allows spatial optimization to incorporate not only geometric characteristics but also occupancy intensity and service-criticality dimensions [10,36].

Table 2 details the specific parameters. High-demand zones (e.g., laboratories) receive maximum service coefficients (D_i = 1.0) to reflect bandwidth-intensive applications, while transient zones (corridors) are weighted lower. These parameters remain constant across all simulations to ensure performance differences are attributable solely to placement and interference coordination strategies, rather than demand bias.

Table 2. User–Demand weighting parameters for functional zones.

Zone Type	User Density (U_i)	Service Coefficient (D_i)	Normalized Weight (w_i)
High Demand (Lab)	25–30	1.00	0.90–1.00
Standard Areas (Classrooms)	20–25	0.75	0.65–0.85
Administrative Offices	5–10	0.25	0.15–0.30
Circulation (Corridors, Lobbies)	10–15	0.40	0.30–0.45

2.3. Material-Aware Indoor Signal Propagation and SINR Modeling

Signal propagation is modeled using a log-normal path loss formulation consistent with ITU-R P.1238-14 [19], enhanced to capture cumulative wall and inter-floor attenuation [14,22]:

$$PL(d) = PL(d_0) + 10n \log_{10}\left(\frac{d}{d_0}\right) + \sum_{k=1}^{N} WAF_k + L_f \quad (2)$$

where $PL(d_0)$ is the reference path loss at d_0 = 1 m, n is the indoor part loss exponent, $\Sigma_k WAF_k$ represents material-specific partition losses (e.g., brick, concrete), and L_f denotes reinforced-concrete slab attenuation.

Network quality is evaluated using Signal-to-Interference-plus-Noise Ratio (SINR), Received Signal Strength Indicator (RSSI), explicitly accounting for CCI from 3D spatial neighbors. Table 3 summarizes the radio-frequency (RF) parameters, selected to reflect a standard enterprise-grade WLAN deployment.

Physical environmental fidelity is ensured by employing literature-validated WAF for reinforced concrete exterior walls and brick internal partitions. Furthermore, the service threshold (τ) of -67 dBm and the design margin (M) of 6 dB align with the high connectivity reliability targets expected from modern enterprise WLANs. This parametric framework ensures that network performance analyses remain independent of environmental and hardware variables, allowing a focused evaluation of placement and coordination strategies.

Table 3. Indoor Propagation and RF Parameters.

Parameter	Symbol/Value	Source/Justification
Reference distance	d_0 = 1 m	Standard indoor reference distance [14]
Reference path loss	PL(d) = 46 dB	ITU-R P.1238-14 indoor model [19]
Path loss exponent	n = 2.8–3.2	Mixed indoor public buildings [19,20]
Transmit power	P_{tx} = 20 dBm	Typical enterprise WLAN configuration [40]
Transmit antenna gain	G_{tx} = 2 dBi	Ceiling-mounted AP antenna
Receive antenna gain	G_{rx} = 0 dBi	Mobile user device
External wall attenuation	WAF_{eff} = 12–15 dB	Reinforced concrete walls [19,41]
Internal wall attenuation	WAF_{eff} = 4–6 dB	Brick masonry/partitions [19]
Floor slab attenuation	L_f = 18–25 dB	Reinforced concrete floor slabs [14,22]
Miscellaneous losses	L_{misc} = 2 dB	Feeder and implementation margin
Thermal noise power	N_0 = −94 dBm	20 MHz channel, room temperature
RSSI service threshold	τ = −67 dBm	Enterprise WLAN coverage target
Design margin	M = 6 dB	Shadowing and modeling uncertainty

2.4. AP Count Selection Under Coverage and Capacity Constraints

Instead of assuming a fixed AP density, the minimum AP count per floor is determined by the dominant constraint between coverage (N_{cov}) and capacity (N_{cap}):

$$N = \max\left(N_{cov}, N_{cap}\right) \tag{3}$$

In this context, using a target service threshold $\tau = -67$ dBm consistent with enterprise guidance [4], the effective service radius r is derived from the link budget:

$$r = d_0 \cdot 10^{\frac{P_{tx}+G_{tx}+G_{rx}-\tau-PL(d_0)-\sum WAF-L_f-L_{misc}-M}{10n}} \tag{4}$$

To account for corridor–room segmentation, an area efficiency factor, $\eta_A \in (0, 1)$, is applied:

$$N_{cov} = \left\lceil \frac{A_{floor}}{\eta_A \cdot \pi \cdot r^2} \right\rceil \tag{5}$$

To establish a realistic and justifiable traffic load profile, peak user demand U_{max}, concurrency factor α, and per-user bandwidth target R_u, are defined in strict alignment with industry-standard high-density enterprise WLAN design guidelines (e.g., Cisco/Aruba high-density planning principles). The required floor capacity proxy and subsequent AP count are calculated as [18,20]:

$$R_{req} = U_{max} \cdot \alpha \cdot R_u \tag{6}$$

To provide methodological transparency regarding the capacity proxy calculations, the relationship between the simulated SINR values and the achievable throughput is fundamentally governed by the Modulation and Coding Scheme (MCS). Table 4 illustrates a representative mapping based on IEEE 802.11 standards [42], demonstrating how improved SINR translates to higher-order modulation, thereby increasing spectral efficiency.

Under high network traffic conditions, assuming a conservative effective AP capacity (C_{AP}), the capacity-oriented AP requirement N_{cap} is determined as follows:

$$N_{cap} = \left\lceil \frac{R_{req}}{C_{AP}} \right\rceil \tag{7}$$

where C_{AP} represents the conservative effective capacity of an AP under dense traffic. It is critical to note that the capacity metrics utilized in this framework serve as a theoretical spectral efficiency proxy. Rather than executing a full MAC-layer CSMA/CA protocol

simulation, the model employs an SINR-to-MCS mapping approximation to strictly isolate the geometric impact of network topology without overclaiming PHY-layer dynamics.

Table 4. Representative mapping of SINR thresholds to MCS.

Minimum SINR (dB)	Modulation	Coding Rate	Efficiency/Impact
<10	BPSK	1/2	Minimum basic connectivity
≥10	QPSK	1/2	Low-tier data rate
≥15	16-QAM	1/2	Mid-tier data rate
≥20	64-QAM	2/3	High-tier data rate
≥25	64-QAM	5/6	Very high data rate
≥30	256-QAM	3/4	Peak spectral efficiency

Table 5 summarizes the physical, service, and traffic-related parameters used to determine the minimum feasible number of APs per floor under joint coverage and capacity constraints. Unlike conventional density-based planning approaches that assume fixed AP counts, this study derives the deployment density analytically from propagation-aware coverage limits and peak traffic requirements.

Table 5. Parameters and derived bounds for AP count determination per floor.

Item	Symbol/Value	Notes (Assumption)
Floor dimensions	$L \times W = 60 \times 20$ m	Public-service standard floor
Floor area	$A_{\text{floor}} = 1200$ m^2	Derived from floor dimensions
Service RSSI threshold	$\tau = -67$ dBm	Enterprise WLAN coverage target
Tx power/antenna gains	$P_{\text{tx}} = 20$ dBm	Typical enterprise AP configuration
Path loss exponent	$n = 3.0$	Indoor mixed environment [16,24]
Effective WAF	$\Sigma WAF_{\text{eff}} = 18$ dB	Worst-case room-edge penetration
Floor slab attenuation	$L_{\text{f}} = 20$ dB	Reinforced concrete floor slabs [18,19]
Miscellaneous losses	$L_{\text{misc}} = 2$ dB	Feeder and implementation margin
Design margin	$M = 6$ dB	Shadowing and modeling uncertainty
Derived service radius	$r \approx 7.1$ m	From RSSI constraint from link budget
Area efficiency factor	$\eta_{\text{A}} = 0.55$	Corridor–room topology inefficiency
Coverage-based AP bound	N_{cov}	Dominant constraint $\lceil \text{A}/(\eta_{\text{A}} \cdot \pi \cdot r^2) \rceil$ From Equation (5)
Maximum users per floor	$U_{\max} = 100$	Peak public building occupancy [40]
Concurrent activity	$\alpha = 0.5$	Conservative peak activity [40]
Per-user target	$R_{\text{u}} = 5$ Mbps	Digitalization service requirement
Required floor throughput	$R_{\text{req}} = 250$ Mbps	$(U_{\max} \cdot \alpha \cdot R_{\text{u}})$ From Equation (6)
Effective AP capacity	$C_{\text{AP}} = 120$ Mbps	Dense WLAN conservative estimate
Capacity-based AP bound	N_{cap}	$\lceil R_{\text{req}}/C_{\text{AP}} \rceil$ From Equation (7)
Minimum feasible AP count	N_{AP}	$\max(N_{\text{cov}}, N_{\text{cap}})$
Search margin	$\Delta = 10$	Practical over-provisioning range
Evaluated AP range	N	Simulation search space

2.5. User-Centric Placement via Weighted-Centroid (WC) Strategy

To align infrastructure with actual usage, AP positions are computed using a weighted centroid operator over the demand nodes assigned to each service region V_{k}:

$$c_{\text{k}} = \frac{\sum_{i \in V_{\text{k}}} w_i \text{p}_i}{\sum_{i \in V_{\text{k}}} w_i} \tag{8}$$

where $\text{p}_i = (\text{x}_i, y_i, z_i)$ represents the coordinates of the i-th demand node. Unlike geometric symmetry, this strategy shifts APs toward high-demand zones (e.g., laboratories),

effectively creating a demand-driven spatial partitioning analogous to Voronoi-based cell decomposition [25,43].

2.6. 3D VSA for Inter-Floor CCI Mitigation

In multi-story buildings, vertical AP alignment creates structured interference channels due to slab leakage [14,22]. The proposed VSA mitigates this by applying a deterministic horizontal displacement between consecutive floors:

$$c_k^{(f+1)} = (x_k + \Delta x, y_k + \Delta y, z_f + h) \tag{9}$$

where h is floor height and (Δx, Δy) is selected to disrupt vertical alignment while preserving floor-level coverage. This transforms architectural repeatability into a controllable parameter, spatially redistributing interference without requiring additional hardware or transmit power [38].

2.7. Energy-Aware Operation via Load-Aware AP Sleep Scheduling

To further reduce operational energy, an AP enters sleep mode when both user load (U_k) and traffic demand (T_k) fall below service thresholds (Uth, Tth):

$$U_k(t) < U_{th} \;\; and \;\; T_k(t) < T_{th} \tag{10}$$

Crucially, sleep mode is only authorized if neighboring APs can cover the offloaded nodes with $\tau = -67$ dBm. The total annual energy consumption (E_{WLAN}) is calculated based on the sum of the annual operational durations of all APs in active and sleep states (t_k^{act},t_k^{slp}):

$$E_{WLAN} = \sum_{k=1}^{N} \left(P_{act} \cdot t_k^{act} + P_{slp} \cdot t_k^{slp} \right) \tag{11}$$

In this model, P_{act} represents the active operational power of an enterprise-grade AP, while P_{slp} denotes the power consumption in sleep mode. To establish a realistic baseline, power consumption parameters are explicitly defined by synthesizing standard 802.11ax (Wi-Fi 6) hardware specifications with empirical power consumption profiles for enterprise WLAN deployments. While high-density access points feature a maximum Power over Ethernet (PoE+) budget of 25.5 W [44], comprehensive empirical studies on enterprise APs demonstrate that average active transmission states operate near 18 W, and idle or deep sleep states reduce consumption to approximately 6 W [45]. Therefore, the average operational states are conservatively modeled as P_{act} = 18 W and P_{slp} = 6 W.

It is important to clarify that this energy model assumes binary states (active/sleep) without granular partial load adaptation. Transition overheads, such as wake-up costs and control-plane signaling, are approximated as a static efficiency loss to avoid overcomplicating the PHY-layer assumptions. The fundamental objective of this formulation is to demonstrate that the overall energy reduction is driven by two distinct contributors: the initial topological consolidation (deploying fewer total APs via the WS-VSA framework) and the subsequent dynamic sleep scheduling during off-peak hours. This operational layer aligns with energy-aware networking concepts that emphasize system-level coordination for measurable energy savings [9,38].

2.8. Carbon Emission and Cost Analysis Models

The framework translates operational energy and hardware decisions into sustainability metrics. Annual operational carbon emissions ($CO_{2,\,\mathrm{WLAN}}$), operational expenditure ($OPEX_{\mathrm{WLAN}}$), and capital expenditure ($CAPEX_{\mathrm{WLAN}}$) are calculated as:

$$CO_{2,\mathrm{WLAN}} = E_{\mathrm{WLAN}} \cdot EF \tag{12}$$

$$OPEX_{\mathrm{WLAN}} = E_{\mathrm{WLAN}} \cdot p_{\mathrm{e}} \tag{13}$$

$$CAPEX_{\mathrm{WLAN}} = N_{\mathrm{AP}} \cdot C_{\mathrm{HC}} \tag{14}$$

where EF is the regional grid emission factor [11], p_{e} is the unit electricity price, and C_{HC} is the unit hardware cost. This direct translation aligns network planning with low-carbon development goals [3,4].

It is important to note that the energy consumption values calculated in this study are intended for comparative evaluation between deployment strategies rather than serving as absolute predictive metrics for real-world energy billing. The model explicitly isolates the topological efficiency of the WLAN infrastructure, providing a rigorous relative baseline to demonstrate the operational carbon reduction potential of the proposed WS-VSA framework.

2.9. Evaluation Metrics and Statistical Protocol

A multidimensional evaluation structure was established to quantify radio performance and sustainability. Table 6 defines the Key Performance Indicators (KPIs).

To ensure robustness against log-normal shadowing and stochastic user distributions, all experiments were repeated over 50 independent Monte Carlo runs. Results are reported using median and interquartile range (IQR) to provide distribution-resilient estimates, with the median-performing seed selected for visualization.

Table 6. KPIs for radio performance and sustainability evaluation.

Metric	Symbol/Indicator	Primary Objective
Coverage ratio	CR (RSSI $\geq \tau$)	Minimum connectivity assurance
Signal quality	SINR (P10, P50)	Interference robustness and fairness
Service capability	Capacity proxy (mean, P90)	Relative throughput comparison
Hardware efficiency	N_{AP} count	Infrastructure consolidation and CAPEX savings
Operational energy	E_{WLAN}	Building-scale energy performance
Carbon emissions	$CO_{2,\mathrm{WLAN}}$	Environmental impact, Annual CO_2 emissions (kg)
Operating cost	$OPEX_{\mathrm{WLAN}}$	Operational operating cost management, Annual electricity cost ($)

3. Results

This section presents a comparative assessment between the proposed Energy-Aware WS–VSA framework and the traditional corridor-aligned Baseline deployment. The evaluation covers radio performance, interference robustness, and sustainability outcomes, reported as median statistics over 50 independent Monte Carlo simulations to ensure stochastic robustness.

3.1. Probabilistic Analysis of RSSI and SINR Distributions

To assess spatial stability, Empirical Cumulative Distribution Functions (ECDF) were computed for RSSI and SINR across all demand nodes. Table 7 summarizes the key statistical differentials between the Baseline and WS-VSA strategies.

Table 7. Comparative Radio Performance Statistics (Median values over 50 runs).

Metric	Indicator	Baseline	WS–VSA	Improvement
Coverage	Ratio (RSSI ≥ -67 dBm)	97.55%	97.95%	+0.40%
Signal Strength	Median RSSI	-54.2 dBm	-51.8 dBm	+2.4 dB
Interference	SINR P10 (Edge Users)	17.66 dB	25.53 dB	+7.87 dB
	SINR P50 (Median Users)	28.40 dB	34.10 dB	+5.70 dB

As illustrated in Figure 2, both strategies satisfy the enterprise-grade service constraint (RSSI ≥ -67 dBm) with coverage ratios exceeding 97%. However, the WS-VSA framework exhibits a distinct rightward shift in the distribution. Specifically, the median RSSI (P50) improves from -56.6 dBm to -54.6 dBm, as explicitly annotated on the curves. This improvement stems from the demand-weighted centroid placement, which relocates APs from geometric centers toward functional zones, effectively reducing material-induced shadowing and eliminating marginal signal regions (dead zones).

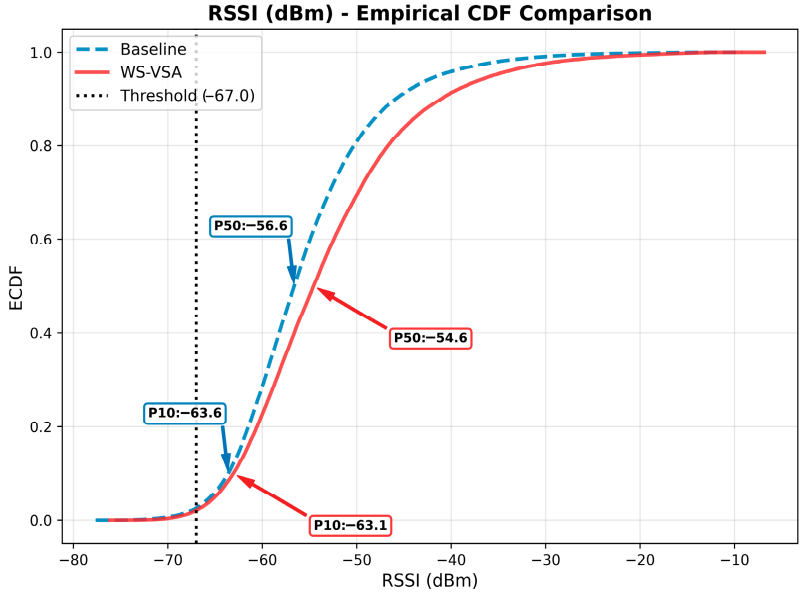


Figure 2. ECDF of RSSI (dBm) with 10th percentile (P10) and median (P50) annotations. The WS-VSA strategy reduces the left-tail mass, indicating fewer dead zones compared to the Baseline.

The SINR analysis, in Figure 3, reveals the most critical performance gain. Unlike RSSI, which shows marginal improvement, SINR demonstrates a structural transformation in network quality. As indicated by the numerical annotations, the WS-VSA framework achieves a substantial +7.7 dB increase in the 10th percentile (P10) edge-user value (from 17.7 dB to 25.4 dB) and an even larger gain in the median (P50) value (from 27.4 dB to 36.1 dB). Furthermore, a Mann–Whitney U test confirms that this improvement is statistically significant ($p < 0.05$) with a Rank–Biserial Correlation of 0.461, indicating a practically large effect size. This confirms that the vertical staggering mechanism effectively disrupts structured inter-floor interference channels without requiring power escalation. By improving edge-user fairness and spatial uniformity, the proposed framework enhances spectral efficiency solely through topological coordination.

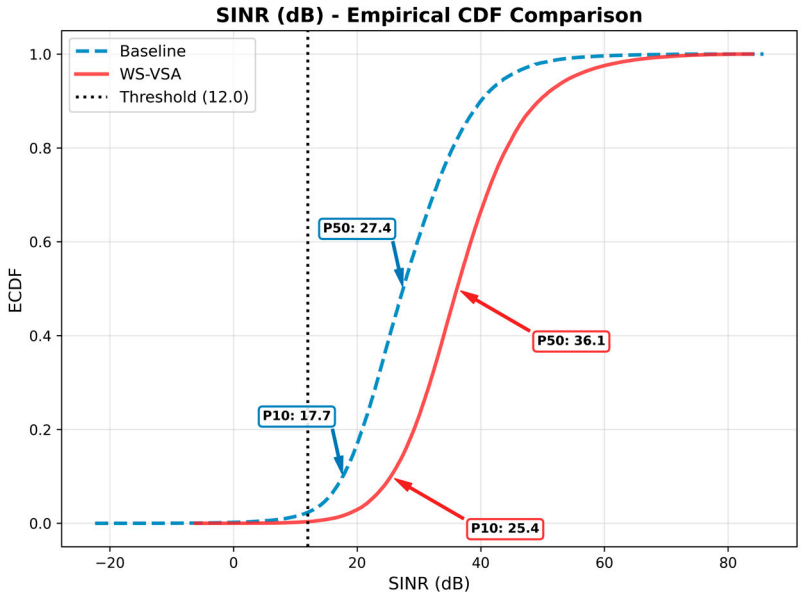


Figure 3. ECDF of SINR (dB) highlighting P10 and P50 values. The pronounced shift in the WS-VSA curve underscores significant gains in interference robustness.

3.2. Optimization Convergence and SINR P10 Stability Analysis

Scalability in dense WLANs is determined not by average signal strength, but by the stability of lower-percentile performance under increasing infrastructure density. Figure 4 illustrates the variation in $SINR_{P10}$ (10th percentile robustness) as a function of AP count per floor.

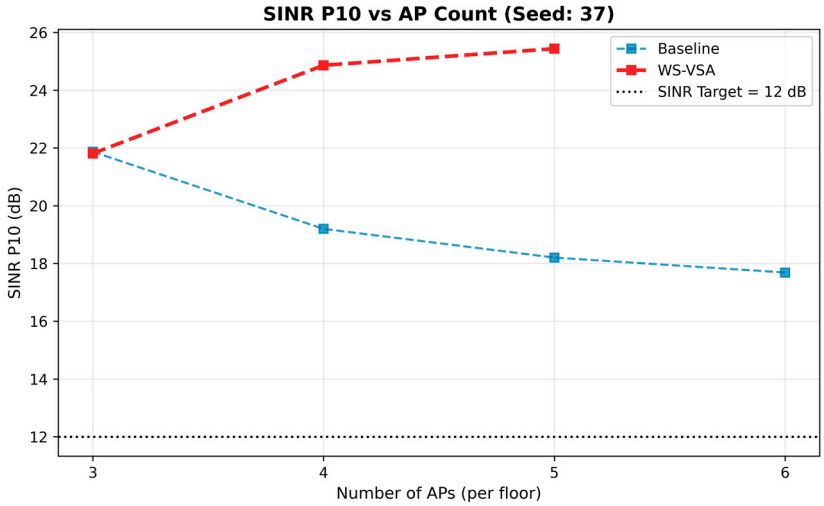


Figure 4. SINR P10 versus AP count per floor for Baseline and WS–VSA strategies. The horizontal dashed line denotes the minimum SINR requirement (12 dB).

A critical divergence emerges as AP density increases. The Baseline configuration exhibits a declining trend, dropping from ~21.8 dB (N = 3) to ~17.7 dB (N = 6). This confirms that geometric symmetry drives the network into an interference-limited regime, where additional APs amplify CCI more rapidly than they improve signal power due to shrinking spatial reuse distances.

In contrast, the WS-VSA framework consistently improves or stabilizes performance, peaking at ~25.5 dB (N = 5). This resilience stems from two coordinated mechanisms:

1. Demand-Driven Gain: The WS component shifts APs toward functional zones, boosting effective signal strength for active users.

2. Interference Decoupling: The VSA component applies horizontal offsets between floors, disrupting vertical interference channels and preventing structured inter-floor CCI accumulation.

Consequently, the proposed framework converts densification into measurable capacity growth rather than interference amplification. This demonstrates that spatial coordination, not merely hardware densification, is the dominant lever for scalable multi-story WLAN performance.

3.3. Relationship Between Coverage Probability and AP Count

Infrastructure density directly dictates both capital and operational costs. Figure 5 illustrates the coverage convergence (RSSI ≥ -67 dBm) as a function of AP count per floor.

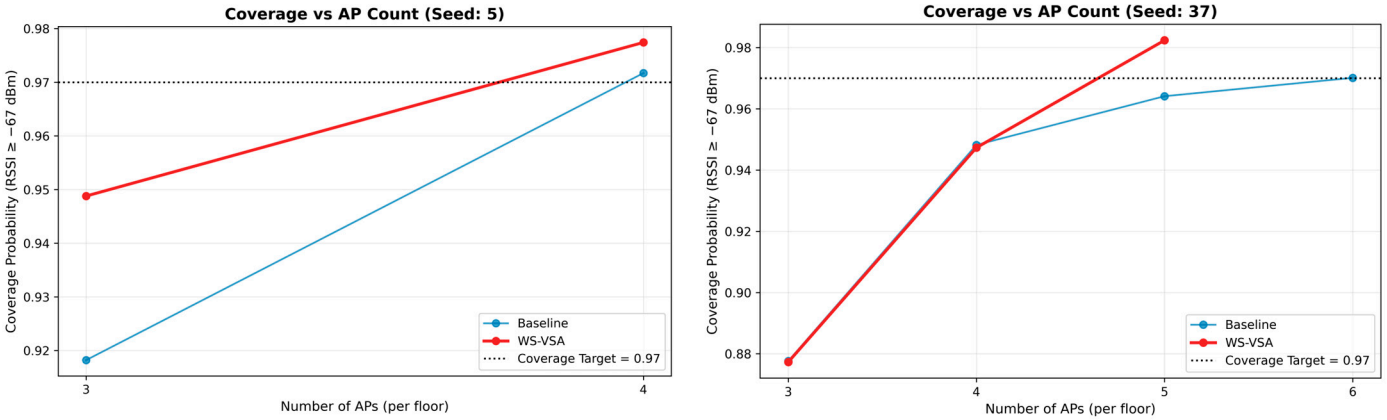


Figure 5. Coverage probability (RSSI ≥ -67 dBm) versus AP count per floor. The dashed horizontal line represents the 97% coverage target.

While both strategies exhibit monotonic growth, their convergence efficiency differs significantly. The Baseline strategy requires a median of 6 APs per floor (18 total) to satisfy the 97% coverage target. In contrast, the WS-VSA framework achieves the same reliability with only 5 APs per floor (15 total). This 16.7% reduction in hardware density (3 fewer APs building-wide) is driven by two structural mechanisms:

1. Minimized Wall Attenuation: Unlike corridor-aligned placement, the WS component positions APs near demand centroids, reducing the average cumulative wall loss between APs and users.
2. Reduced Redundant Overlap: The strategy redistributes excessive signal overlap from circulation areas to functional shadow regions, maximizing the effective coverage area per AP.

Crucially, this efficiency is achieved without increasing transmit power. By satisfying identical Quality of Service (QoS) constraints with fewer devices, the framework reduces both CAPEX and standby power consumption, establishing the physical foundation for the energy and carbon savings detailed in Section 3.8.

3.4. Spatial Distribution Analysis: RSSI and SINR Heatmaps

To investigate the physical drivers behind the statistical improvements, per-floor RSSI and SINR heatmaps were generated. These visualizations map signal propagation and interference patterns within the building envelope.

The Baseline deployment Figure 6 exhibits elongated corridor-aligned lobes. Signal penetration into peripheral rooms is hindered by wall attenuation, creating localized sub-threshold pockets near the service boundary ($\tau = -67$ dBm). In contrast, the WS-VSA strategy positions APs at the weighted centroids of functional zones. This topology

minimizes wall-crossing penalties and originates signal propagation from within high-occupancy rooms rather than circulation paths. Consequently, structural elements act as cell separators rather than obstacles, resulting in a more homogeneous field distribution.

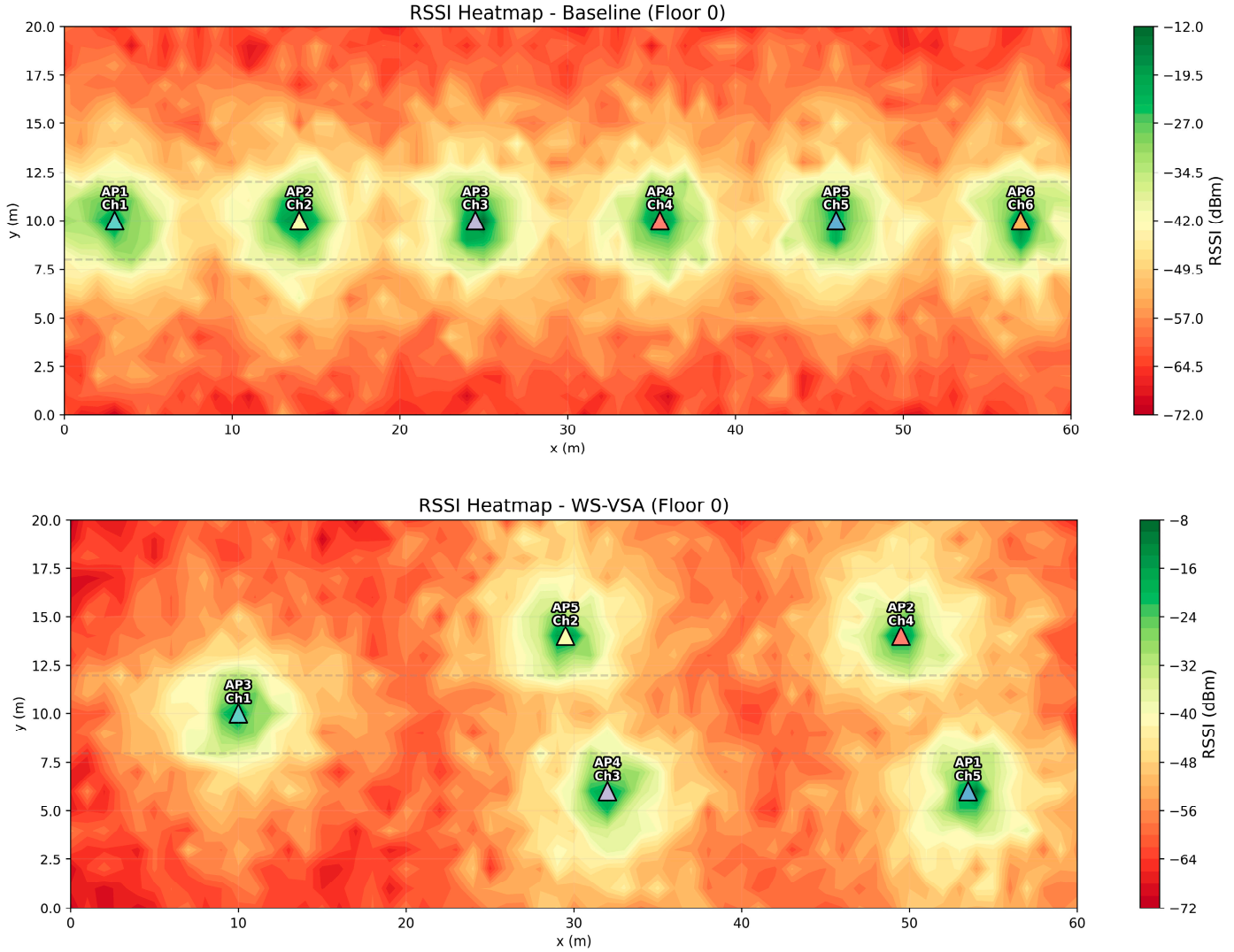


Figure 6. RSSI (dBm) heatmaps for Floor 0 under both the Baseline and WS-VSA strategies. The dashed horizontal lines represent the corridor boundaries and internal wall structures.

Figure 7 illustrates the critical impact of vertical coordination. In the Baseline configuration, vertically aligned APs create structured CCI zones, evident as cool-colored low-SINR regions in the building core. Even with slab attenuation, the geometric symmetry enforces interference coupling.

Conversely, the WS-VSA framework disrupts this symmetry via deterministic horizontal staggering (Section 2.6). As shown in Figure 7, this spatial decorrelation expands high-SINR regions (warm colors) across the floor. This visual confirmation explains the statistical rise in $SINR_{P10}$ to 25.53 dB reported in Section 3.1. By converting architectural segmentation into a spatial reuse advantage, the proposed framework achieves spectral cleanliness without increasing hardware intensity.

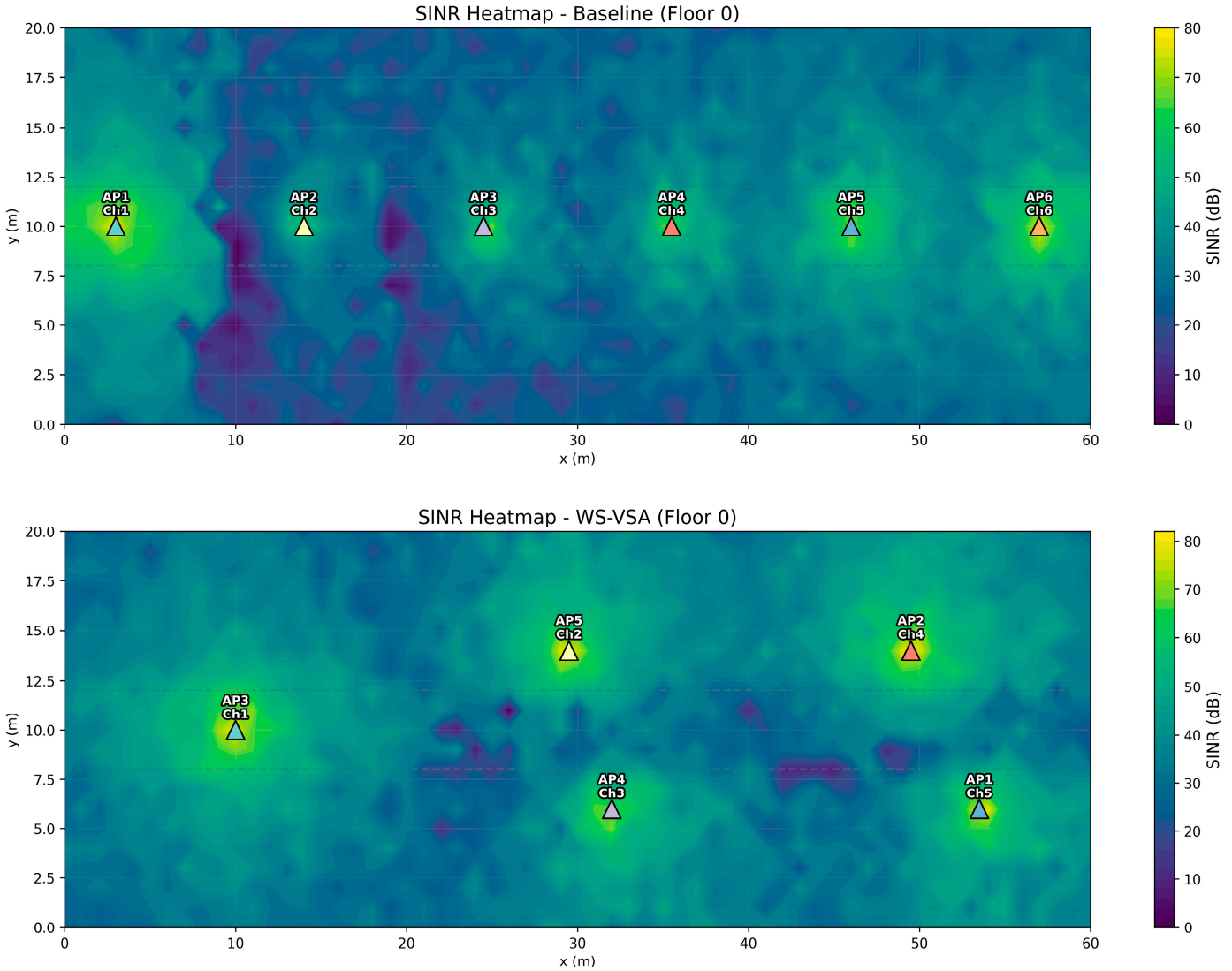


Figure 7. Floor-0 SINR (dB) heatmaps for Baseline and WS-VSA methods. The dashed horizontal lines represent the corridor boundaries and internal wall structures.

3.5. Spectral Visibility and Interference Behavior

In dense indoor environments, the number of simultaneously visible APs is a critical determinant of contention and spectral reuse. While coverage requires at least one dominant AP, excessive multi-AP visibility (RSSI ≥ -67 dBm) increases airtime competition and interference coupling. Figure 8 presents the spectral visibility maps for Floor 0.

In Figure 8, in the Baseline (top), a continuous "interference corridor" is created, while WS-VSA (bottom) uses walls for spectral isolation. In the Baseline configuration, the linear alignment of APs creates a continuous "interference corridor" along the central axis. This geometric regularity results in extended longitudinal overlap zones where three or more APs are simultaneously visible. This high-density visibility effectively compresses the available clean spectrum and directly explains the suppressed SINR P10 (17.66 dB) observed in Section 3.1.

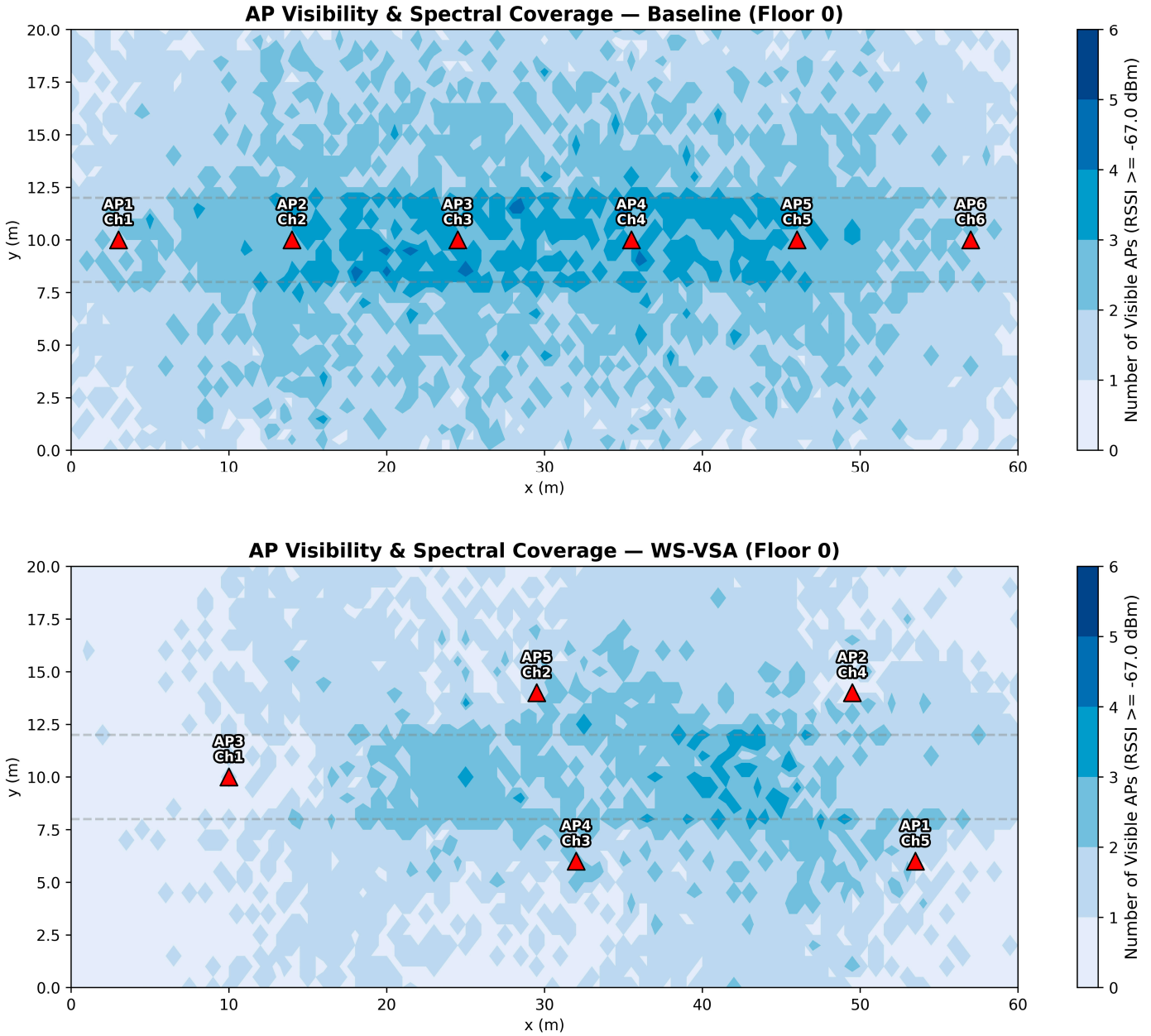


Figure 8. AP visibility and spectral coverage analysis for Floor-0: Comparison between Baseline and WS-VSA methods. The dashed horizontal lines represent the corridor boundaries and internal wall structures.

Conversely, the WS-VSA deployment utilizes weighted functional centroids and vertical staggering to spatially redistribute overlap. Rather than concentrating visibility along a single axis, it creates a segmented spectral structure where structural walls and floor slabs serve as natural isolation boundaries. The reduction in high-order visibility regions (locations with $\geq$3 visible APs) indicates improved spatial reuse.

While the Baseline pushes the network toward an interference-limited regime as density grows, WS-VSA maintains controlled overlap boundaries. This geometric visibility control provides the physical explanation for the 30.6% increase in capacity proxy and the energy efficiency gains summarized in Table 8.

Table 8. Building-Wide Performance Comparison (Median over 50 Seeds).

Metric	Baseline	WS-VSA	Relative Change (%)
AP Count (Per Floor/Total)	6/18	5/15	−16.7%
Coverage Probability (≥ -67 dBm)	97.55%	97.95%	+0.4%
Robustness SINR P10 (dB)	[CI: 16.9–18.4] 17.66	[CI: 24.8–26.1] 25.53	+44.6%
Average Capacity Proxy (Mbps)	84.62	110.54	+30.6%
Annual CO_2 Emissions (kg)	838.23	590.83	−29.5%
Annual Energy Consumption (kWh)	1892.16	1333.71	−29.5%
Annual OPEX ($)	378.43	266.74	−29.5%

3.6. Three-Dimensional Topology and Volumetric SINR Behavior

In multi-story public buildings, vertical signal leakage significantly influences spectral efficiency. To quantify this, a 3D evaluation was conducted to assess the geometric impact of AP topology on volumetric SINR distribution.

Figure 9 contrasts the deployment geometries. The Baseline configuration creates a "stacked" alignment, where APs share identical horizontal coordinates across floors. Given the limited attenuation of reinforced concrete slabs (18–25 dB), this minimizes the effective separation distance and maximizes vertical coupling. Conversely, the WS-VSA strategy (Section 2.6) forces inter-floor signals to traverse diagonal paths by introducing deterministic horizontal staggering. This elongation of the interference path reduces coupling without modifying transmit power.

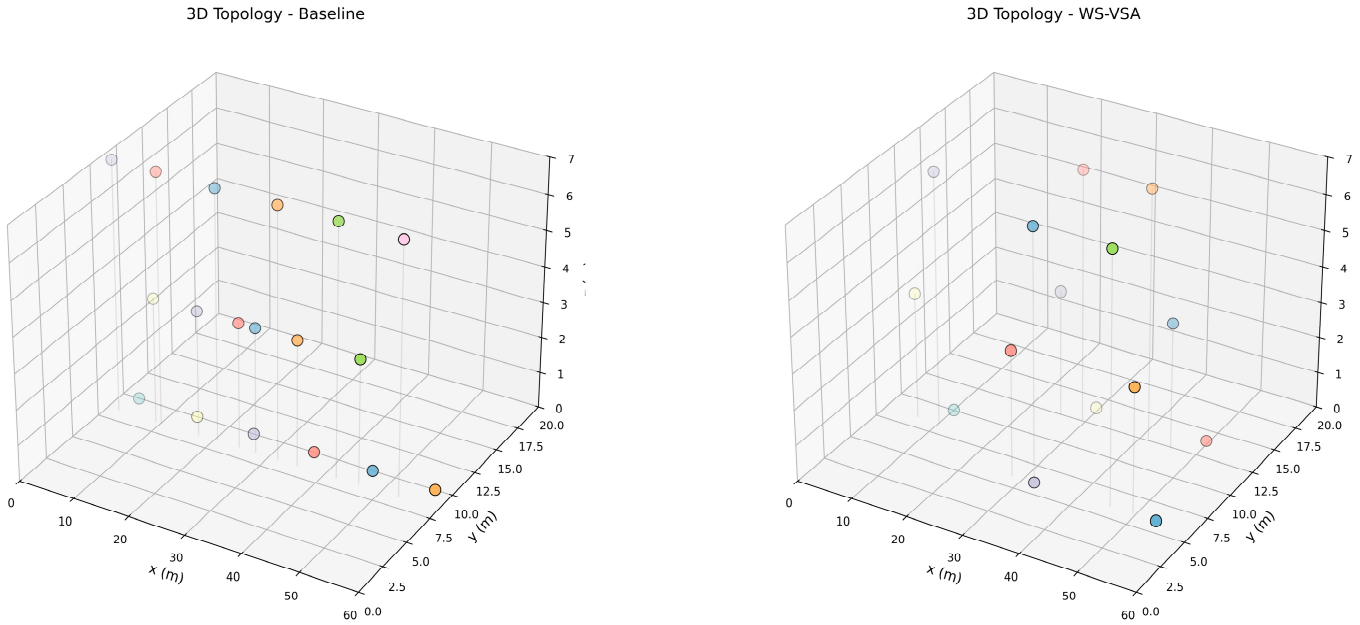


Figure 9. 3D AP deployment topology for Baseline and WS-VSA methods. The different colors of the nodes represent the various Wi-Fi channel assignments used to minimize co-channel interference within the 3D building environment.

The consequence of this topological shift is visualized in Figure 10. The Baseline exhibits distinct "interference columns" in the central core, severely constraining volumetric spectral reuse. The WS-VSA framework eliminates these artifacts, producing a spatially continuous high-SINR volume. This geometric mitigation translates directly into the +7.87 dB gain in lower-percentile performance, with SINR P10 also rising from 17.66 dB to 25.53 dB. By distributing interference heterogeneously, the framework ensures scalable densification without transitioning into an interference-dominated regime.

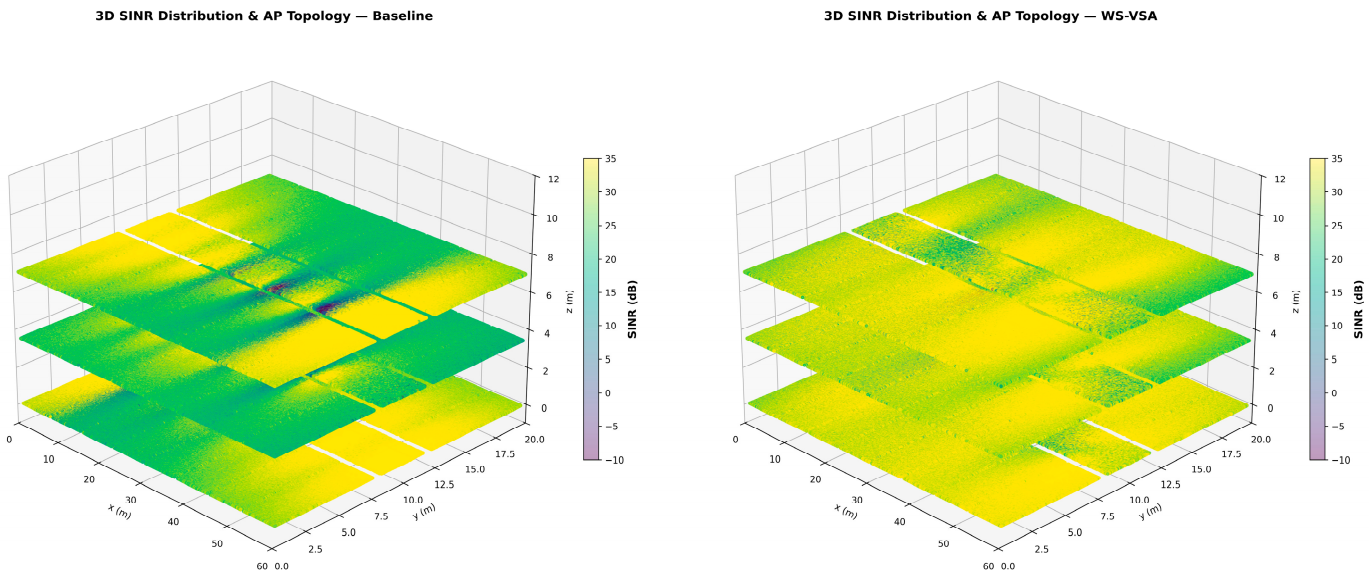


Figure 10. 3D volumetric SINR distribution for Baseline and WS-VSA methods.

3.7. System-Level Capacity and Throughput Analysis

Network capacity is the ultimate metric of spectral efficiency. Figure 11 quantifies the system-level throughput gain derived from the 50 simulation scenarios.

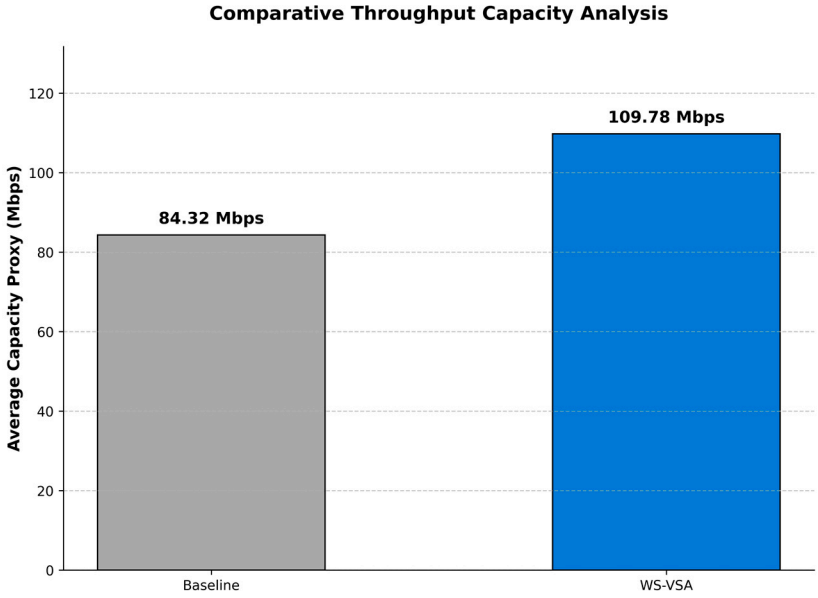


Figure 11. Comparison of average system-level network capacity for Baseline and WS-VSA methods (bar heights represent median performance).

The WS-VSA framework delivers a median capacity of 110.54 Mbps, representing a significant 30.6% net increase over the Baseline (84.62 Mbps). This gain is driven by the lowered spectral interference floor (improved SINR). By reducing the noise floor, the VSA strategy allows Adaptive Modulation and Coding mechanisms to select higher-order MCS. Consequently, the network achieves a radical improvement in data transmission performance while operating under strict energy-efficiency constraints.

3.8. Sustainability Impacts: Energy, Carbon, and Economic Analysis

The aggregated building-wide performance of the proposed WS-VSA framework is summarized in Table 8. These results, derived from the median of 50 Monte Carlo runs,

quantify the simultaneous gains in spectral efficiency and operational sustainability. To ensure statistical rigor for log-normal shadowing environments, Table 8 includes the 95% Confidence Intervals (CI) for key stochastic metrics. Furthermore, a Mann–Whitney U test confirms that the improvement in SINR P10 distribution under WS-VSA is statistically significant ($p < 0.05$).

As illustrated in Figure 12, simulation results confirm that, even with similar initial coverage targets, the WS-VSA strategy reduces annual carbon emissions from 838.2 kg CO_2 to 590.8 kg CO_2. This calculation utilizes a regional Emission Factor (EF $\cong$ 0.44 kg CO_2/kWh) reflecting the national electricity grid average in Türkiye, effectively contextualizing the reference building scenario. In parallel with this environmental improvement, annual OPEX decreased from $378.4 to $266.7.

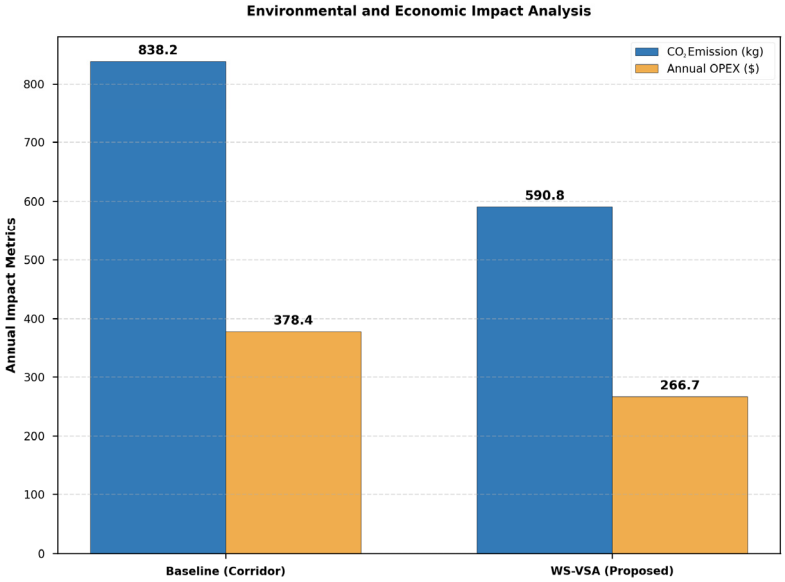


Figure 12. Comparison of annual carbon emissions and operational expenditures for Baseline and WS-VSA approaches.

This represents a consistent 29.5% reduction across energy, carbon, and cost metrics. When combined with the infrastructure consolidation (16.6% lower CAPEX due to fewer APs), the WS-VSA framework demonstrates that intelligent, topology-aware digital infrastructure planning actively supports low-carbon transition pathways in public buildings without requiring physical retrofitting.

Regarding operational energy demand, Figure 13 highlights the consumption differences between the two strategies. Under the Baseline configuration, maintaining coverage continuity requires continuous active operation, resulting in an annual demand of 1892.2 kWh. In contrast, the WS-VSA framework leverages demand density control to reduce this annual consumption to 1333.7 kWh.

This translates to an absolute energy saving of approximately 558.5 kWh per year for the modeled three-story facility. While this absolute value represents a smaller fraction of a building's total thermal load (e.g., HVAC systems), it constitutes a highly cost-effective 24/7 operational baseload optimization.

This 29.5% net reduction is achieved without service degradation; notably, it is accompanied by a 44.6% increase in SINR robustness. This confirms that energy savings are driven by intelligent spatial coordination rather than by sacrificing network quality.

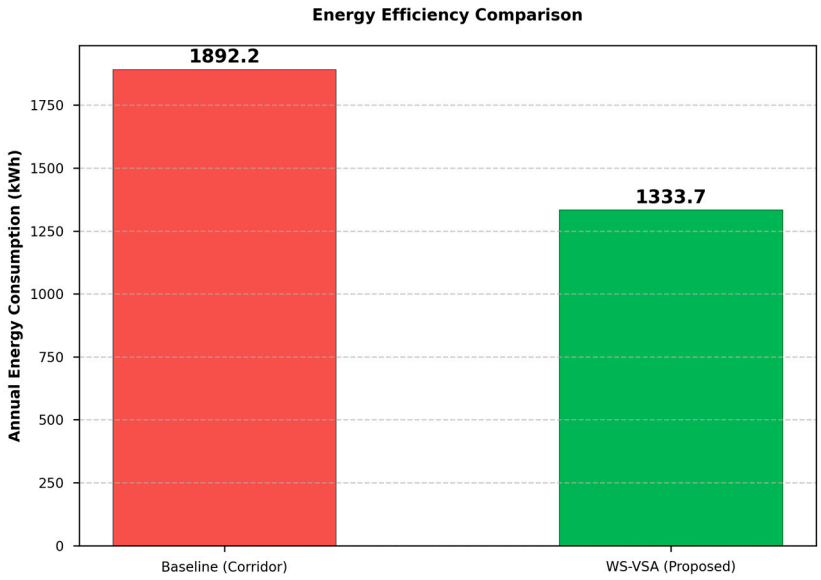


Figure 13. Comparison of annual energy consumption across scenarios.

4. Discussion

This study evaluates WLAN deployment as a building-integrated energy optimization problem rather than a purely communication-oriented layout task. The findings demonstrate that spatial coordination and demand-aware scheduling can simultaneously improve spectral efficiency and reduce operational energy consumption in multi-story public buildings.

4.1. Energy–QoS Relationship Under Spatial Optimization

A common assumption in green networking literature is that energy savings require performance trade-offs, such as reduced transmit power or aggressive sleep scheduling [5,8,38]. However, the results of this study indicate a different regime. The WS-VSA framework achieved a 29.5% reduction in annual energy consumption while simultaneously increasing the median SINR P10 by 44.6%. This outcome suggests that interference-aware spatial placement reduces retransmission overhead and improves spectral reuse efficiency. Consequently, energy reduction is not achieved by throttling network resources, but by mitigating interference-induced inefficiencies. This aligns with system-level energy coordination principles [9], where architectural restructuring often yields larger benefits than isolated device-level optimization [46].

4.2. Interference Geometry and Vertical Decoupling

The Baseline deployment's vertically aligned geometry exacerbates inter-floor coupling, as floor slab attenuation alone provides insufficient isolation [14,22]. The proposed VSA mechanism introduces deterministic horizontal offsets, effectively increasing the interference path length and leveraging material attenuation. The observed +7.87 dB improvement in SINR P10 confirms that vertical decoupling is a major driver of spectral robustness. Unlike power-control [28] or sleep-only mechanisms [29], this strategy modifies network geometry rather than transmission parameters, ensuring interference suppression without sacrificing coverage continuity.

4.3. Environmental Implications in Building Energy Context

Building energy optimization studies increasingly incorporate digital infrastructure into the operational ecosystem [1,2,13]. To contextualize the practical relevance of these results, it is essential to compare the WLAN energy savings with primary building energy

consumers like Heating, Ventilation, and Air Conditioning (HVAC) systems. While the absolute annual energy reduction achieved by the WS-VSA framework (~558.5 kWh) is orders of magnitude smaller than seasonal HVAC loads, the WLAN infrastructure represents a persistent, 24/7 operational baseload. Unlike thermal optimization strategies (e.g., window glazing or HVAC tuning), which fluctuate heavily based on external climate conditions and thermal inertia, WLAN spatial optimization is entirely climate-independent. This unique characteristic ensures that the 29.5% reduction in operational energy is permanently achieved without requiring any physical retrofitting, making it a highly cost-effective and globally transferable intervention. These findings support the argument that digital network topology must be integrated into holistic building energy management strategies [47], particularly through early-stage Building Information Modeling (BIM) design and dynamic integration with Building Energy Management Systems (BEMS) via standard API interfaces for off-peak load scheduling.

4.4. Generalizability to Asymmetric Floor Plans

To demonstrate the robustness and generalizability of the proposed WS-VSA framework beyond symmetrical geometries, an additional stress-test scenario featuring an irregular floor plan was simulated. In this scenario, the corridor was shifted off-center, creating asymmetrical room dimensions across the building's longitudinal axis.

As shown in Figure 14, the algorithm successfully adapted to the structural irregularity without any manual intervention. The demand-weighted placement dynamically redistributed the optimum number of APs (N = 7) to accommodate the varying zone capacities, while the vertical staggering mechanism maintained strict inter-floor interference control. This validates that the spatial optimization principles of the WS-VSA framework are architecturally adaptable and highly effective in real-world, heterogeneous public buildings.

4.5. Quantitative Sensitivity Analysis

A quantitative sensitivity analysis was conducted to evaluate the stability of the WS-VSA framework under varying environmental and operational parameters. As presented in Table 9, the impact of ±20% variations in the WAF, maximum user density, and AP power consumption was tested on the representative seed.

Table 9. Quantitative sensitivity analysis of the WS-VSA framework under ±20% variations in WAF, maximum user density, and AP power consumption.

Parameter Variation	SINR P10 (dB)	Throughput (Mbps)	Annual Energy (kWh)
Baseline (WS-VSA)	24.56	108.68	1111.42
WAF +20%	25.31	110.97	1111.42
WAF −20%	23.66	106.09	1111.42
User Density ±20%	24.56	108.68	1111.42
AP Power +20%	24.56	108.68	1333.71
AP Power −20%	24.56	108.68	889.14

The results indicate that the framework is highly robust. Notably, even under a 20% penalty in wall attenuation (WAF +20%), the SINR degradation remains marginal (~0.9 dB), confirming the topological stability of the proposed approach. Furthermore, proportional changes in user density and AP power consumption gracefully scale the throughput and energy metrics without causing network failure or coverage dead zones.

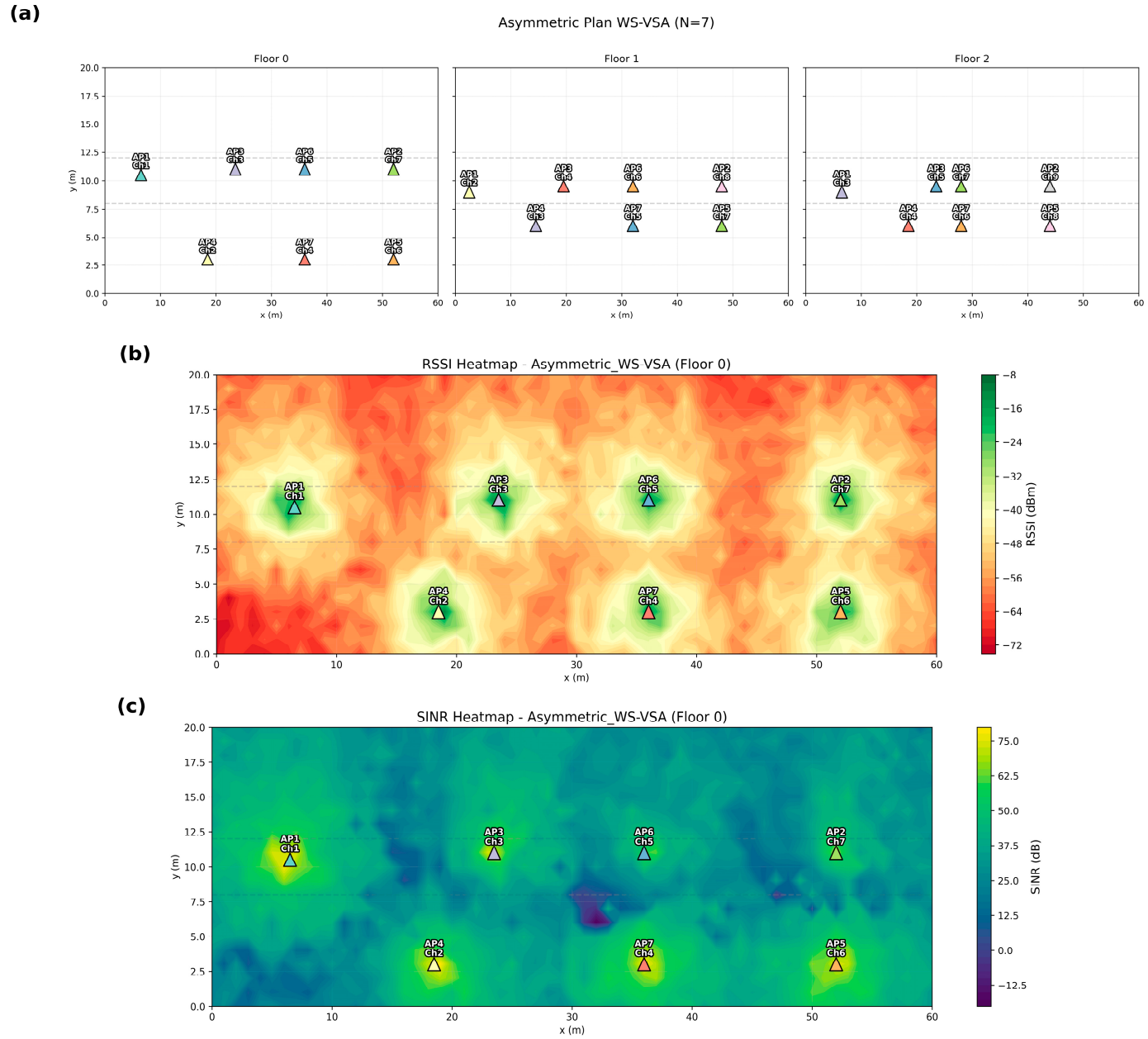


Figure 14. Multi-floor performance evaluation of the proposed WS-VSA framework under a realistic asymmetric building scenario. (**a**) 3D AP layout and channel assignment demonstrating the algorithm's adaptive placement across irregular zone shapes (N = 7). (**b**) The resulting RSSI heatmap on the ground floor (Floor 0), ensuring comprehensive connectivity coverage despite the off-center corridor. (**c**) The corresponding SINR heatmap on the ground floor, proving the effectiveness of the vertical staggering mechanism in mitigating co-channel interference within non-uniform architectural structures. The dashed horizontal lines represent the corridor boundaries and internal wall structures.

4.6. Scalability and Limitations

While the core mechanisms—demand-weighted placement and vertical staggering—are topology-agnostic and transferable to other multi-story buildings, including asymmetric floor plans and varying structural materials, certain limitations exist in this foundational study. Because the primary goal was to mathematically isolate the geometric impact of the vertical staggering algorithm from dynamic environmental noise, a controlled Monte Carlo simulation based on the globally validated ITU-R P.1238-14 model was utilized. Thus, the lack of empirical measurement campaigns constitutes a limitation. The study modeled user mobility stochastically rather than dynamically in real-time and assumed

fixed active/sleep power states without granular PHY-layer adaptation. Additionally, specific Wireless Fidelity (Wi-Fi) 6/7 features (e.g., OFDMA) were not explicitly modeled. Future experimental validation in real-world operational buildings is a critical next step to validate these findings against hardware anomalies and dynamic human body shadowing, further strengthening external validity.

5. Conclusions

This study introduced an Energy-Aware WLAN Deployment Framework (WS-VSA) for multi-story public buildings, integrating demand-weighted spatial placement with vertical interference coordination and load-aware operation. The primary objective was to demonstrate that network topology is not merely a connectivity variable but a critical lever for operational sustainability.

Monte Carlo simulations confirm that the proposed framework shifts WLAN operation from an interference-limited regime toward an energy-efficient state. The WS-VSA strategy reduces annual energy consumption, carbon emissions, and operational expenditures by 29.5%, while simultaneously improving edge-user signal quality (SINR P10) by 7.87 dB and average throughput by 30.6%. Crucially, these gains are achieved while maintaining a coverage reliability of over 97%, proving that energy efficiency does not require a compromise in service quality.

By integrating spatial optimization with radio resource management, this study directly addresses the growing demands within the Green ICT literature for infrastructure-level sustainability interventions [48,49]. Unlike conventional state-of-the-art WLAN optimization schemes that predominantly rely on reactive power scaling or sleep-mode scheduling, the WS-VSA framework demonstrates that strategic, 3D architectural alignment can permanently reduce the operational carbon footprint of digital infrastructures without compromising network performance and reliability.

The key contribution of this work lies in reframing WLAN planning as a building-integrated energy optimization problem. By quantifying the impact of vertical geometric decoupling, this study provides a reproducible framework linking QoS metrics directly to sustainability indicators. Future research will focus on scaling and validating this framework across a larger number of architecturally diverse buildings, integrating this approach with Wi-Fi 7 Multi-Link Operation, developing real-time occupancy-aware adaptive deployment algorithms, and coupling WLAN optimization with HVAC-aware digital twin platforms and BEMS to further advance the zero-emission building paradigm.

Funding: This research received no external funding.

Data Availability Statement: All simulation data generated during this study are available from the corresponding author upon reasonable request.

Conflicts of Interest: The authors declare no conflicts of interest.

Abbreviations

The following abbreviations are used in this manuscript:

WS	Weighted Spatial
VSA	Vertical Staggering Algorithm
WS-VSA	Weighted Spatial with Vertical Staggering Algorithm
CCI	Co-Channel Interference
WLAN	Wireless Local Area Network
WAF	Wall Attenuation Factors

RF	Radio Frequency
RSSI	Received Signal Strength Indicator
SINR	Signal-to-Interference-plus-Noise Ratio
AP	Access Point
OPEX	Operational Expenditure
CAPEX	Capital Expenditure
KPI	Key Performance Indicator
ECDF	Empirical Cumulative Distribution Functions
QoS	Quality of Service
Wi-Fi	Wireless Fidelity
OFDMA	Orthogonal Frequency Division Multiple Access
HVAC	Heating, Ventilation, and Air Conditioning
MCS	Modulation and Coding Scheme
PoE+	Power over Ethernet

References

1. Ascione, F.; Bianco, N.; De Stasio, C.; Mauro, G.M.; Vanoli, G.P. Simulation-based model predictive control by the multi-objective optimization of building energy performance. *Energy Build.* **2016**, *111*, 131–148. [CrossRef]
2. Cheekatamarla, P.K. Energy-efficient building technologies. In *Advanced Nanomaterials and Their Applications in Renewable Energy*, 2nd ed.; Elsevier: Amsterdam, The Netherlands, 2022; pp. 3–33. [CrossRef]
3. Hu, J.; Zhang, H.; Irfan, M. How does digital infrastructure construction affect low-carbon development? A multidimensional interpretation of evidence from China. *J. Clean. Prod.* **2023**, *396*, 136467. [CrossRef]
4. Aslan, J.; Mayers, K.; Koomey, J.G.; France, C. Electricity intensity of internet data transmission: Untangling the estimates. *J. Ind. Ecol.* **2017**, *22*, 785–798. [CrossRef] [PubMed]
5. Dahal, M.S.; Shrestha, J.N.; Shakya, S.R. Energy saving technique and measurement in green wireless communication. *Energy* **2018**, *159*, 21–31. [CrossRef]
6. Arnold, O.; Richter, F.; Fettweis, G.; Blume, O. Power consumption modeling of different base station types in heterogeneous cellular networks. In Proceedings of the Future Network & Mobile Summit, Florence, Italy, 16–18 June 2010. Available online: https://ieeexplore.ieee.org/document/5722444 (accessed on 10 January 2026).
7. Marsan, M.A.; Chiaraviglio, L.; Ciullo, D.; Meo, M. Optimal energy savings in cellular access networks. In Proceedings of the IEEE International Conference on Communications Workshops, Dresden, Germany, 14–18 June 2009. [CrossRef]
8. Han, T.; Ansari, N. Powering mobile networks with green energy. *IEEE Wirel. Commun.* **2014**, *21*, 90–96. [CrossRef]
9. Rault, T.; Bouabdallah, A.; Challal, Y. Energy efficiency in wireless sensor networks: A top-down survey. *Comput. Netw.* **2014**, *67*, 104–122. [CrossRef]
10. Naji, N.; Abid, M.R.; Krami, N.; Benhaddou, D. Energy-aware wireless sensor networks for smart buildings: A review. *J. Sens. Actuator Netw.* **2021**, *10*, 67. [CrossRef]
11. Coşar, M. Carbon footprint in data center: A case study. *Fresenius Environ. Bull.* **2012**, *28*, 600–607.
12. Karbasforoushha, M.A.; Khajehzadeh, M.; Jearsiripongkul, T.; Keawsawasvong, S.; Eslam, M. A comprehensive review of building energy optimization using metaheuristic algorithms. *J. Build. Eng.* **2024**, *98*, 111377. [CrossRef]
13. Shi, Y.; Zheng, S.; Gao, D.; Yang, X. Multi-objective optimization of embodied carbon emission, energy consumption, and daylighting performance of educational building in the schematic design stage. *J. Build. Eng.* **2025**, *106*, 112594. [CrossRef]
14. Seidel, S.Y.; Rappaport, T.S. 914 MHz path loss prediction models for indoor wireless communications in multifloored buildings. *IEEE Trans. Antennas Propag.* **1992**, *40*, 207–217. [CrossRef]
15. Anderson, H.R. (Ed.) *Fixed Broadband Wireless System Design*; John Wiley & Sons: Hoboken, NJ, USA, 2003; 512p.
16. Pahlavan, K.; Levesque, A.H. *Wireless Information Networks*, 2nd ed.; John Wiley & Sons: Hoboken, NJ, USA, 2005; 752p.
17. Rappaport, T.S. *Wireless Communications: Principles and Practice*, 2nd ed.; Prentice Hall: Upper Saddle River, NJ, USA, 2024. [CrossRef]
18. Keenan, J.M.; Motley, A.J. Radio coverage in buildings. *Br. Telecom Technol. J.* **1990**, *8*, 19–24.
19. ITU-R. *Recommendation ITU-R P.1238-14: Propagation Data and Prediction Methods for Indoor Radiocommunication Systems*; International Telecommunication Union: Geneva, Switzerland, 2021. Available online: https://www.itu.int/rec/R-REC-P.1238 (accessed on 3 April 2026).
20. Kang, T.; Seo, J. Practical simplified indoor multiwall path-loss model. In Proceedings of the 20th International Conference on Control, Automation and Systems (ICCAS), Busan, Republic of Korea, 13–16 October 2020. [CrossRef]

21. Segun, A.A.; Isaac, F.I.; Atilade, A.G. Effects of building materials and structures on indoor path loss of very high frequency radio wave. *Am. J. Eng. Res. (AJER)* **2022**, *11*, 73–80.
22. Yang, W.; Zhang, J.; Song, H.; Zhang, J. Partition-based analytic evaluation of building wireless performance. *IEEE Trans. Veh. Technol.* **2021**, *70*, 9036–9049. [CrossRef]
23. Mogensen, P.E.; Wigard, J. *COST Action 231: Digital Mobile Radio Towards Future Generation System, Final Report*; European Commission: Brussels, Belgium, 1999.
24. Yang, W.; Zhang, J.; Glazunov, A.A.; Zhang, J. Line-of-sight probability for channel modeling in 3-D indoor environments. *IEEE Antennas Wirel. Propag. Lett.* **2020**, *19*, 1182–1186. [CrossRef]
25. Amaldi, E.; Capone, A.; Cesana, M.; Filippini, I.; Malucelli, F. Optimization models and methods for planning wireless access networks. *Comput. Netw.* **2008**, *52*, 2159–2171. [CrossRef]
26. Farkas, K.; Husrak, A.; Godor, G. Optimization of Wi-Fi Access Point Placement for Indoor Localization. *Inform. It Today* **2013**, *1*, 28–33.
27. Chen, L.; Xu, F.; Jin, K.; Tang, Z. Energy-saving access point configurations in WLANs: A swarm intelligent approach. *J. Supercomput.* **2023**, *79*, 19332–19364. [CrossRef]
28. Qiao, D.; Choi, S.; Shin, K.G. Energy-efficient WLAN operation via transmit power control. *Comput. Netw.* **2003**, *42*, 175–198. [CrossRef]
29. Nedevschi, S.; Popa, L.; Iannaccone, G.; Ratnasamy, S.; Wetherall, D. Reducing network energy consumption via sleeping and rate adaptation. In *Proceedings of the 5th USENIX Symposium on Networked Systems Design and Implementation (NSDI'08)*; USENIX Association: Berkeley, CA, USA, 2008; pp. 323–336.
30. Salahdine, F.; Opadere, J.; Liu, Q.; Han, T.; Zhang, N.; Wu, S. A survey on sleep mode techniques for ultra-dense networks in 5G and beyond. *Comput. Netw.* **2022**, *201*, 108567. [CrossRef]
31. Qui, S.; Chu, X.; Leung, Y.W.; Ng, J.K.Y. Joint access point placement and power-channel-resource-unit assignment for 802.11ax-based dense WiFi with QoS Requirements. In *IEEE INFOCOM 2020—IEEE Conference on Computer Communications*; IEEE: Piscataway, NJ, USA, 2020; pp. 1038–1051. [CrossRef]
32. Yang, W.; Zhang, J.; Zhang, J. Machine learning based indoor line-of-sight probability prediction. In *2019 International Symposium on Antennas and Propagation (ISAP)*; IEEE: Piscataway, NJ, USA, 2019; pp. 1–3.
33. López-Ramírez, G.A.; Aragón-Zavala, A. Enhancing indoor mmWave communication with ML-based propagation models. *IEEE Access* **2025**, *13*, 13748–13769. [CrossRef]
34. Lee, S.-H.; Cheng, C.-H.; Huang, T.-H.; Huang, Y.-F. Machine Learning-based Indoor Positioning Systems Using Multi-Channel Information. *J. Eng. Technol. Sci.* **2023**, *55*, 373–383. [CrossRef]
35. Zhang, J.; Glazunov, A.A.; Yang, W.; Zhang, J. Fundamental wireless performance of a building. *IEEE Wirel. Commun.* **2022**, *29*, 186–193. [CrossRef]
36. Hu, X.; Assaad, R.H. A BIM-enabled digital twin framework for real-time indoor environment monitoring and visualization. *J. Build. Eng.* **2024**, *86*, 108901. [CrossRef]
37. Khazaeli, M.A.; Javadpour, L.; Lindholm, E.; Estrada, H.; Lee, L.S. Wi-Fi analysis using building information modeling. In Proceedings of the IISE Annual Conference and Expo, New Orleans, LA, USA, 20–23 May 2022. Available online: https://scholarlycommons.pacific.edu/esob-facpres/603 (accessed on 10 January 2026).
38. Cao, X.; Liu, L.; Cheng, Y.; Shen, X. Towards energy-efficient wireless networking in the big data era: A survey. *IEEE Commun. Surv. Tutor.* **2018**, *20*, 303–332. [CrossRef]
39. Alvarado, R.; Suárez, A. A novel energy-saving method for campus wired and dense WiFi network applying machine learning and idle cycling techniques. *FACETS* **2024**, *9*, 1–19. [CrossRef]
40. Cisco Systems. Enterprise Mobility 8.5 Design Guide: High-Density Deployment (Cisco White Paper). 2024. Available online: https://www.cisco.com/c/dam/en/us/td/docs/wireless/controller/technotes/8-5/cisco-enterprise-mobility-design-guide-8-5.pdf (accessed on 10 January 2026).
41. Aileen, A.; Suwardi, A.D.; Prawiranata, F. WiFi signal strength degradation over different building materials. *Eng. Math. Comput. Sci. J. (EMACS)* **2021**, *3*, 109–113. [CrossRef]
42. *IEEE Std 802.11bf-2025 (Amendment to IEEE 802.11-2024)*; IEEE Standard for Information Technology—Telecommunications and Information Exchange Between Systems Local and Metropolitan Area Networks—Specific Requirements—Part 11: Wireless LAN Medium Access Control (MAC) and Physical Layer (PHY) Specifications—Amendment 4: Enhancements for Wireless LAN Sensing. IEEE: Piscataway, NJ, USA, 2025; pp. 1–228. [CrossRef]
43. Arif, M.; Wyne, S.; Nawaz, A.J. Indoor localization using Voronoi tessellation. *Adv. Electr. Comput. Eng.* **2018**, *18*, 85–90. [CrossRef]
44. Cisco Systems. Cisco Catalyst 9120AX Series Access Points Data Sheet. 2023. Available online: https://www.cisco.com/c/en/us/products/collateral/wireless/catalyst-9120ax-series-access-points/datasheet-c78-742115.html (accessed on 24 March 2026).
45. Silva, P.; Almeida, N.T.; Campos, R. A Comprehensive Study on Enterprise Wi-Fi Access Points Power Consumption. *IEEE Access* **2019**, *7*, 96841–96867. [CrossRef]

46. Bianzino, A.P.; Chaudet, C.; Rossi, D.; Rougier, J.-L. A Survey of Green Networking Research. *IEEE Commun. Surv. Tutor.* **2012**, *14*, 3–20. [CrossRef]
47. Dmytriyeva, K. Smart Building Technology: Revolutionizing Modern Infrastructure. 2025. Available online: https://www.cim.io/blog/smart-building-technology-revolutionizing-modern-infrastructure (accessed on 10 January 2026).
48. Almudayni, Z.; Soh, B.; Samra, H.; Li, A. Energy Inefficiency in IoT Networks: Causes, Impact, and a Strategic Framework for Sustainable Optimisation. *Electronics* **2025**, *14*, 159. [CrossRef]
49. Safitra, M.F.; Lubis, M.; Lubis, A.R.; Alhari, M.I. The Need for Energy-Efficient Networks: A Review of Green Communication Systems and Network Architectures. In *Intelligent Sustainable Systems. WorldS4 2023; Lecture Notes in Networks and Systems*; Nagar, A.K., Jat, D.S., Mishra, D., Joshi, A., Eds.; Springer: Singapore, 2024; Volume 803. [CrossRef]

Disclaimer/Publisher's Note: The statements, opinions and data contained in all publications are solely those of the individual author(s) and contributor(s) and not of MDPI and/or the editor(s). MDPI and/or the editor(s) disclaim responsibility for any injury to people or property resulting from any ideas, methods, instructions or products referred to in the content.